INCORPORATION OF SPATIAL CONSTRAINTS INTO SPECTRAL MIXTURE ANALYSIS OF REMOTELY SENSED HYPERSPECTRAL DATA

Antonio Plaza, Javier Plaza and Gabriel Martín

Department of Technology of Computers and Communications
University of Extremadura, Avda. de la Universidad s/n, E-10071 Cáceres, SPAIN
E-mail: {aplaza, jplaza, gamahe}@unex.es

ABSTRACT

Spectral mixture analysis is an important technique to analyze remotely sensed hyperspectral data sets. This approach involves the separation of a mixed pixel into its pure components or *endmember* spectra, and the estimation of the abundance value for each endmember. Several techniques have been developed for extraction of spectral endmembers and estimation of fractional abundances. However, an important issue that has not been yet fully accomplished is the incorporation of spatial constraints into endmember extraction and, particularly, fractional abundance estimation. Another relevant topic is the use of nonlinear versus linear mixture models, which can be unconstrained or constrained in nature. Here, the constraints refer to non-negativity and sum to unity of estimated fractional abundances for each pixel vector. In this paper, we investigate the impact of including spatial and abundance-related constraints in spectral mixture analysis of remotely sensed hyperspectral data sets. For this purpose, we discuss the advantages that can be obtained after including spatial information in techniques for endmember extraction and fractional abundance estimation, using a database of synthetic hyperspectral scenes with artificial spatial patterns generated using fractals, and a real hyperspectral scene collected by NASA's Airborne Visible Infra-Red Imaging Spectrometer (AVIRIS).

1. INTRODUCTION

Spectral unmixing has been an alluring exploitation goal since the earliest days of imaging spectroscopy [1]. No matter the spatial resolution, in natural environments, spectral signatures in hyperspectral data are invariably a mixture of the signatures of the various materials found within the spatial extent of the ground instantaneous field view [2]. Due to the high spectral dimensionality of the data, the number of spectral bands usually exceeds the number of spectral mixture components, and the unmixing problem is cast in terms of an over-determined system of equations in which, given a correct set of pure spectral signatures called *endmembers* in the hyperspectral imaging literature [3].

Since each observed hyperspectral signal is generally the result of an actual mixing process, the driving abundances are often required to satisfy two constraints. First, all abundances must be non-negative. Second, the sum of abundances for a given pixel must be unity [4]. However, it is the derivation and validation of the correct suite of endmembers that has remained a challenging and elusive goal for the past several years.

Several approaches have been developed for automatic or semi-automatic endmember extraction, including the pixel purity index (PPI) algorithm [5], the orthogonal subspace projection (OSP) [6], the N-FINDR algorithm [7], or the iterative error analysis (IEA) algorithm [8], among others [3]. Although these methods have shown considerable promise, they are exclusively based on the spectral information of the data. However, most endmember extraction algorithms could benefit from an integrated framework in which both the spectral information and the spatial arrangement of pixel vectors are taken into account. It should be noted that the inclusion of spatial information in the spectral unmixing problem is not limited to the endmember extraction stage. Even after a suite of spectral *endmembers* has been derived from the input data, the estimation of their fractional abundances at sub-pixel levels can also take advantage of the existing spatial autocorrelation among image features. Although the information related with spatial context has been widely used in full-pixel classification approaches [9], it has been seldom used in sub-pixel analysis.

In this paper, we address this issue and further develop a technique which incorporates the spatial information into both endmember extraction and spectral unmixing. The proposed technique relies on the linear mixture model, and can be implemented by assuming that the abundances are either constrained or unconstrained. This approach is compared to other spectral-based approaches for spectral unmixing, using both simulated and real hyperspectral data sets. To conclude the paper, we briefly address the nonlinear spectral unmixing problem using machine learning techniques, and the impact of abundance constraints in this case.

978-1-4244-4948-4/09/$25.00 © 2009 IEEE

2. INCORPORATION OF SPATIAL INFORMATION INTO SPECTRAL MIXTURE ANALSYIS

In this section, we develop an approach for endmember extraction and spectral unmixing which incorporates spatial constraints in both stages. The algorithm makes use of classic morphological operations of erosion and dilation [10], which have been extended to hyperspectral data via the introduction of an ordering relationship among pixel vectors in the data. The main idea of the algorithm is to impose an ordering relation in terms of spectral purity in the set of pixels lying within a spatial search window (structuring element) around each image pixel vector. To do so, we first define a cumulative distance between a particular pixel vector $\boldsymbol{f}(x,y)$, i.e., an N-dimensional vector at discrete spatial coordinates (x,y), and all the pixel vectors in the spatial neighborhood given by B (B-neighborhood) as follows:

$$D_B(\boldsymbol{f}(x,y)) = \sum_{(i,j)\in Z^2(B)} Dist(\boldsymbol{f}(x,y),\boldsymbol{f}(i,j)), \quad (1)$$

where (i,j) are the spatial coordinates of the pixels in the B-neighborhood discrete domain, represented by $Z^2(B)$, and *Dist* is a pointwise distance measure between two N-dimensional vectors. In this work, we use the spectral information divergence (SID) as the baseline distnace measure. The SID is based on the concept of divergence, and obtains the discrepancy of probabilistic behaviors between two spectral signatures designated by $\boldsymbol{f}_i = [f_{i1}, f_{i2}, ..., f_{in}]$ and $\boldsymbol{f}_j = [f_{j1}, f_{j2}, ..., f_{jn}]$. Here it is important to emphasize that the term 'spectral signature' does not necessarily imply 'pixel vector'. Subsequently, the spatial coordinates (x,y) have been omitted from the two spectral signatures above to simplify our formulation, although the following argument would be the same if two pixel vectors were considered. If we assume that the two signatures above are made up of non-negative entries (which is a reasonable assumption in imaging spectroscopy data), then two probabilistic measures can be respectively defined as follows:

$$M[f_{ik}] = p_k = f_{ik} / \sum_{l=1}^{N} f_{il}, \quad M[f_{jk}] = p_k = f_{jk} / \sum_{l=1}^{N} f_{jl} \quad (2)$$

Using the above definitions, the self-information provided by $\boldsymbol{f}_j$ for band l is given by $I_l(\boldsymbol{f}_j) = -log\ q_l$. We can further define the entropy of $\boldsymbol{f}_j$ with respect to $\boldsymbol{f}_i$ by:

$$\begin{aligned} D(\boldsymbol{f}_i \| \boldsymbol{f}_j) &= \sum_{l=1}^{N} p_l\ D_l(\boldsymbol{f}_i \| \boldsymbol{f}_j) \\ &= \sum_{l=1}^{N} p_l (I_l(\boldsymbol{f}_j) - I_l(\boldsymbol{f}_i)) = \sum_{l=1}^{N} p_l\ log(p_l/q_l) \end{aligned} \quad (3)$$

By means of equation (3), SID is defined as follows:

$$\text{SID}(\boldsymbol{f}_i,\boldsymbol{f}_j) = D(\boldsymbol{f}_i \| \boldsymbol{f}_j) + D(\boldsymbol{f}_j \| \boldsymbol{f}_i) \quad (4)$$

With the above definitions in mind, a description of the proposed endmember extraction and spectral unmixing algorithm is given below. The algorithm, based on the automated morphological endmember extraction (AMEE) [10], allows propagation of pure pixels between subsequent iterations, and also incorporates a spatial/spectral unmixing stage which was not present in the previous version.

The inputs to the algorithm are the full hyperspectral data cube $\boldsymbol{f}$, a structuring element B (used to define the spatial context around each image pixel), a maximum number of algorithm iterations I_{max}, and a number of endmembers to be extracted, p. The output is an endmember set, $\{\boldsymbol{e}_i\}_{i=1}^{q}$, with $q \leq p$. The algorithm consists of the following steps:

1. Set $i = 1$ and initialize a morphological eccentricity index $\text{MEI}(x,y) = 0$ for each pixel $\boldsymbol{f}(x,y)$.

2. Move B through all the pixels of the input data, defining a local spatial search area around each pixel $\boldsymbol{f}(x,y)$, and calculate the maximum and minimum pixel vectors at each B-neighborhood using extended morphological erosion and dilation, which are respectively defined as follows [11]:

$$(\boldsymbol{f} \ominus B)(x,y) = \text{argmin}_{(i,j)\in Z^2(B)}\{D_B[\boldsymbol{f}(x+i, y+j)]\} \quad (5)$$

$$(\boldsymbol{f} \oplus B)(x,y) = \text{argmax}_{(i,j)\in Z^2(B)}\{D_B[\boldsymbol{f}(x+i, y+j)]\} \quad (6)$$

3. Update the MEI at each spatial location (x,y) using:

$$\text{MEI}(x,y) = Dist[(\boldsymbol{f} \ominus B)(x,y), (\boldsymbol{f} \oplus B)(x,y)] \quad (7)$$

4. Set $i = i + 1$. If $i = I_{max}$, then go to step (5). Otherwise, replace the original image with its dilation using B using $\boldsymbol{f} = \boldsymbol{f} \oplus B$. This represents an optimization that propagates only the purest pixels at the local neighborhood to the following algorithm iteration. Then, go to step (2).

5. Select the set of p pixel vectors with higher associated MEI scores (called endmember candidates) and form a unique spectral set of $\{\boldsymbol{e}_i\}_{i=1}^{q}$ pixels, with $q \leq p$, using the OSP algorithm [6] to perform this task.

6. Once a set of p endmembers have been extracted from the input data, a spatial/spectral unmixing procedure is accomplished by considering a spatial neighborhood (defined by B) around each mixed pixel. This method is similar to traditional ones, in the sense that it makes use of the standard (fully constrained or unconstrained) least squares-based technique to estimate

abundance fractions [4]. But it differs from traditional methods in the fact that the endmember set used for each pixel is adaptively calculated based on the spatial context. The method is based on the following steps:

(a) Before unmixing a certain pixel $\boldsymbol{f}(x, y)$, a weight is assigned to the pixels in the B-neighborhood centered at spatial coordinates (x, y) by first calculating, for each pixel in the B-neighborhood, the *Dist* to each one of the endmembers in the set $\{\boldsymbol{e}_i\}_{i=1}^{q}$, and then labeling the pixel as an instance of a certain endmember (candidate) by using the minimum *Dist* score.

(b) Then, a weight is assigned to each endmember candidate (the weight is inversely proportional to the minimum *Dist* score for that candidate).

(c) Finally, all endmember candidates located in the B-neighborhood are sorted by weight, and only those with associated weights above a certain tolerance threshold are incorporated to the 'local' endmember set which is finally used to unmix the pixel $\boldsymbol{f}(x, y)$.

As shown by the algorithm description above, the proposed method is based on the selection of a set of 'local' endmembers at each spatial neighborhood defined by the morphological structuring element. These endmembers are then used to define a MEI score which reflects the degree of spectral purity of signatures at local spatial neighborhoods defined around each image pixel. The pixels with maximum MEI scores are then used to obtain the global endmembers by avoiding endmember repetitions. Therefore, our proposed spatial/spectral endmember extraction method follows a local-to-global approach in the search of image endmembers, and further incorporates spatial constraints in the spectral unmixing stage performed for estimation of endmember fractional abundances.

3. EXPERIMENTAL DATA

3.1. Synthetic hyperspectral data

A database of five synthetic hyperspectral scenes has been created using fractals to generate distinct spatial patterns, which are then used to simulate linear mixtures of reflectance signatures selected from a spectral library compiled by the U.S. Geological Survey (USGS)[1]. Fig. 1 shows the five scenes considered in experiments, and 2 shows the nine fractional abundance maps used in the generation of one of such scenes. In Fig. 2, black color indicates 0% abundance of the corresponding mineral, white color indicates 100% abundance of the mineral, and fractional abundances in each pixel of the scene sum to unity. Zero-mean Gaussian noise was added to the scenes in different signal to noise ratios (SNRs) –from 30:1 to 110:1– to simulate contributions from ambient (clutter) and instrumental sources, following the procedure described in [6].

[1] http://speclab.cr.usgs.gov/spectral-lib.htm

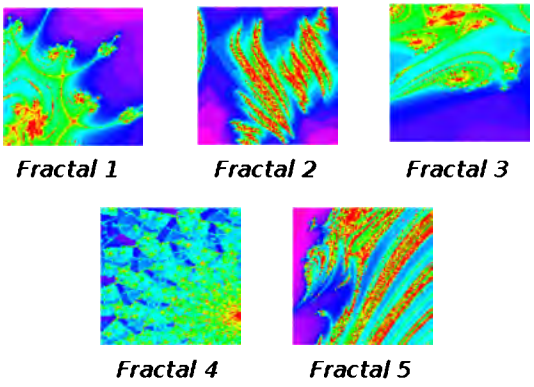

Fig. 1. Synthetic images used in experiments, where spatial patterns where generated using fractals.

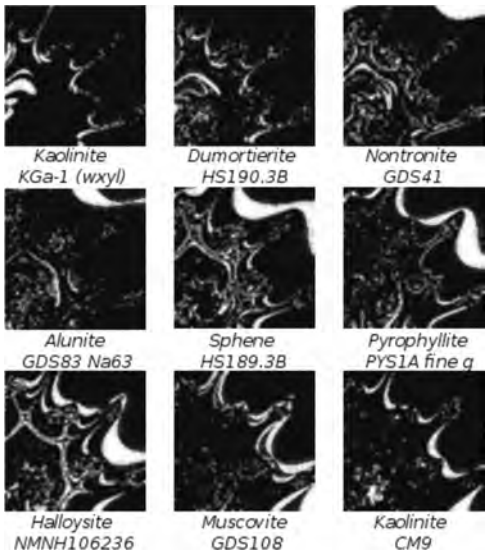

Fig. 2. Fractional abundance distributions used in the generation of one of the synthetic images.

3.2. Real hyperspectral data

A well-known hyperspectral data set has been selected for the purpose of illustrating the spectral unmixing algorithm described in this work. The data set was collected by the AVIRIS sensor over the Cuprite mining district in Nevada [see Fig. 3(a)], and is available online in both radiance and

reflectance units[2]. In our experiments, we use reflectance data in order to relate our results to the reference USGS spectral library. The scene selected for experiments is the one labeled as f970619t01p02_r02_sc03.a.rfl. This scene comprises a relatively large area (350 × 350 pixels and 20-meter pixels) and 224 spectral bands between 0.4 and 2.5 μm. Bands 1-3, 105-115 and 150-170 were removed prior to the analysis due to water absorption and low SNR in those bands. The site is well understood mineralogically, and has several exposed minerals of interest. Fig. 3(b-c) shows reference ground signatures of the above minerals. These signatures will be used to assess endmember signature purity in this work.

4. EXPERIMENTAL RESULTS

4.1. Experiments with synthetic hyperspectral data

We have first conducted an analysis of the proposed spatial/spectral technique in the task of extracting pure spectral signatures from the five synthetic scenes in Fig. 1 with different SNR proportions, and compared the obtained results to those provided by a purely spectral technique such as N-FINDR. In all cases, the number of endmembers to be extracted was set to $p = 9$, the number of random USGS spectral signatures used for the construction of those scenes. In order to ensure the fairest possible comparison, the best performance must be obtained from each alternative method. In this work, we have individually optimized each method to achieve the best possible results (by analyzing different spectral matching criteria) by testing all possible parameter values (within reasonable range values) and report the best result obtained for each algorithm with each considered scene.

Table 1 shows the number of extracted endmembers that were matched (using the spectral similarity matching algorithm described in [3]) to their corresponding reference USGS spectral signatures, along with the mean spectral angle distance (SAD) of the matched endmembers for the proposed algorithm and for the OSP and N-FINDR algorithms, when the algorithms were applied to the five synthetic scenes without noise and with SNRs ranging from 30:1 to 110:1. In the table, lower SAD indicates higher spectral similarity. As shown by Table 1, the spectral-based OSP algorithm provides the best results in terms of matched endmembers and spectral similarity of extracted endmembers with regards to reference USGS signatures in the experiments with synthetic hyperspectral data. On the other hand, the proposed approach outperforms the N-FINDR in terms of average SAD, and performs similarly to N-FINDR in terms of matched endmembers. The proposed method was sensitive to the window size used in morphological operations, but similar results were obtained by using structuring elements ranging from 5×5 to 15×15 pixels. It should be noted that the results reported on Table 1 refer to the spectral similarity of extracted endmembers with regards to reference signatures used in the construction of the synthetic scenes, but do not analyze the quality of fractional abundance estimations resulting from such endmembers. As a result, further experiments are highly desirable in order to evaluate the accuracy of the proposed fractional abundance estimation approach in combination with the endmember extraction stage.

[2]http://aviris.jpl.nasa.gov/html/aviris.freedata.html

Table 1. Number of matched endmembers with regards to USGS reference spectral signatures and average SAD score (in the parentheses) of matched endmembers for each set of $p = 9$ endmembers extracted by OSP, N-FINDR and the proposed spatial/spectral algorithm from the synthetic scenes without noise and with SNRs from 30:1 to 110:1.

Scene	OSP	N-FINDR	Proposed
Fractal1	9.00 (0.004)	7.15 (0.039)	5.82 (0.025)
Fractal2	9.00 (0.002)	5.15 (0.062)	6.00 (0.019)
Fractal3	9.00 (0.010)	6.00 (0.049)	5.57 (0.023)
Fractal4	9.00 (0.008)	5.82 (0.052)	5.00 (0.023)
Fractal5	9.00 (0.015)	5.27 (0.053)	5.28 (0.023)

4.2. Experiments with real hyperspectral data

To illustrate the performance of the proposed spatial/spectral unmixing method with a real hyperspectral scene, we have conducted an experimental assessment of spectral mixture analysis algorithms using the well-known AVIRIS Cuprite data set. In experiments, we have first considered a standard mixed pixel decomposition procedure based on endmember extraction followed by least squares-based linear spectral unmixing [4]. Four algorithms: PPI, N-FINDR, IEA and the proposed spatial/spectral method were considered for comparison purposes. Although in practice it is very difficult to fully optimize each method, we have used our previous experience with these methods to select parameters which are reasonably close to optimal for the test data. For the proposed method, the best results were obtained using a structuring element with 15×15 pixels in size. The parameter values selected are in agreement with those used before in previous studies [3].

In addition, four linear spectral unmixing algorithms were used in this experiment to derive endmember fractional abundances. These include the standard fully constrained (FC) and unconstrained (UC) least-squares based methods, and also two novel methods: spatial/spectral fully constrained (SPFC) and spatial/spectral unconstrained (SPUC) unmixing, presented in this work as the last step of the proposed algorithm (but which can also use endmembers derived by other methods as input). Prior to a full examination and discussion of results, it is important to outline parameter values used for the considered endmember extraction algorithms,

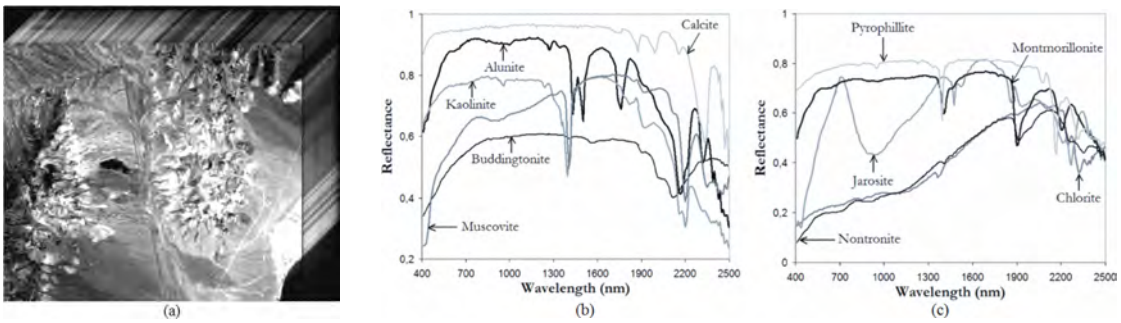

Fig. 3. AVIRIS Cuprite scene (a) and reference spectra for the scene (b-c).

bearing in mind that all of them require that the number of endmembers to be extracted, p, be set as an input parameter.

In this work, we estimate the number of endmembers in the AVIRIS Cuprite data using the virtual dimensionality (VD) concept, which has been shown in previous work to be an effective approach for this purpose [12]. The VD estimated a total of $p = 16$ endmembers, which is consistent with the available ground-truth for the scene. For the PPI algorithm, we used the version available in Research Systems ENVI 4.0 software, which is based on a semi-automatic procedure that first generates a large number of random vectors with unit norm (10^4 in experiments) and then projects the pixel vectors in the data to those random vectors, using ENVI's N-dimensional visualization tool to manually select a final endmember set. For the proposed algorithm, we used a structuring element with size of 3×3 pixels and fixed the value of parameter $I_{max} = 5$.

An experiment-based cross-examination of algorithm endmember extraction accuracy is presented in Table 2, which tabulates the SAD scores obtained after comparing some selected USGS library spectra with the corresponding endmembers extracted by the four considered algorithms. The smaller the SAD values across the ten minerals considered, the better the results. It should be noted that Table 2 only displays the smallest SAD scores of all endmembers with respect to each USGS signature for each algorithm. As shown in the table, all tested methods produced endmembers which were similar, spectrally, to the USGS reference signatures. Interestingly, the SAD spectral similarity scores obtained for the proposed spatial/spectral algorithm were generally very low, and often superior to those reported by spectral-based algorithms. This demonstrated the importance of considering not only spectral but also spatial information in the selection of image endmembers, even when the ultimate goal is to find most spectrally pure signatures (in this case, the incorporation of spatial information directs the endmember search to spatially homogeneous areas, in which it is easier to identify spectrally pure pixels).

It is important to note that the linear mixture model is generally not flexible enough to accommodate the full range

Table 2. SAD-based spectral similarity scores among selected USGS mineral spectra in Fig. 3(b-c) and the endmembers produced by different algorithms.

Mineral	PPI	N-FINDR	IEA	Proposed
Alunite	0.084	0.081	0.084	0.063
Buddingtonite	0.106	0.084	0.112	0.084
Calcite	0.105	0.105	0.093	0.090
Chlorite	0.125	0.136	0.096	0.088
Kaolinite	0.136	0.152	0.134	0.134
Jarosite	0.112	0.102	0.112	0.089
Montmorillonite	0.106	0.089	0.120	0.082
Muscovite	0.108	0.094	0.105	0.077
Nontronite	0.102	0.099	0.099	0.078
Pyrophilite	0.094	0.090	0.112	0.080

of spectral variability throughout real-world landscapes. In order to accurately characterize the data, it might be necessary to account for multiple scattering effects, which overestimate the results obtained from a linear scattering model. In order to calibrate the performance of linear spectral unmixing adopted in this work for estimating sub-pixel fractional abundances in the AVIRIS Cuprite data, we also unmixed the data using the considered FC, UC, SPFC and SPUC algorithms. Interestingly, our experiments revealed that the correspondent endmember fractional abundance maps derived by using SPFC and SPUC were in visual agreement for all endmember extraction methods tested. In addition, negative and/or unrealistic SPUC-derived abundance fractions (which usually indicate a bad fit of the model and reveal inappropriate endmember selections) were very rarely found, in particular, when the proposed spatial/spectral algorithm was used for the endmember selection stage. Quite opposite, the abundance maps derived by the UC algorithm showed a much more significant fraction of negative abundances, in particular, when endmembers were derived using the spectral information only. Having those circumstances in mind, the results in this section indicate that the linear mixture model, improved by the integration of spatial and spectral information, was able to provide a relatively good characterization of complex mixtures in the Cuprite mining district. Further experimentation with nonlinear models is highly desirable to fully substantiate the above remarks.

4.3. Experiments with nonlinearly mixed data

To expand our disscussion to a nonlinear mixing scenario, this subsection briefly discusses the use of machine learning techniques in order to deal with nonlinearly mixed data. For this purpose, we use a multi-layer perceptron neural network in which the neuron count at the input layer, N, equals the number of spectral bands. The number of neurons at the output layer, p, equals the number of spectral endmembers. The number of neurons in the hidden layer is empirically set to the square root of the product of the number of input features and information classes, a configuration shown to be successful in previous work [11].

In order to illustrate the effectiveness of the MLP neural network architecture in nonlinear spectral unmixing, we have considered a database consisting of a set of mineral mixtures with absolute ground truth. The data consisted of 20 spectra collected using RELAB, a bi-directional, high-resolution spectrometer able to collect 211 spectral bands in the spectral range from 0.4 to 2.5 μm. In addition to three spectral endmembers corresponding to minerals *anorthosite*, *enstatite* and *olivine*, the database contains ten binary mixtures and seven ternary mixtures. We first estimated the abundance fractions of pure signatures in the 20 available spectra using the fully constrained (FC) and unconstrained (UC) linear mixture models. From our experiments, we observed that both FC and UC accurately characterized the binary mixtures, but for the ternary mixtures a nonlinear model was required. With this in mind, we trained the MLP architecture using the backpropagation algorithm. Additional training samples were generated from the three pure endmember signatures and the available mixed training samples by artificially adding random noise (according to RELAB sensor SNR characteristics) to the available samples, thus assisting the backpropagation training process. It should be noted that the ground-truth abundance fractions for these spectra were known in advance, thus allowing us to train the MLP architectures with highly mixed training samples. The incorporation of the most highly mixed available samples allowed us to reduce the overall fractional abundance estimation errors in about 6% for the most complex mixtures, indicating that intelligently trained machine learning techniques can accurately learn the structure of complex mixtures for sub-pixel characterization of hyperspectral data.

5. CONCLUSIONS AND FUTURE LINES

In this paper, we have investigated the impact of including spatial and abundance-related constraints in spectral mixture analysis of synthetic and real hyperspectral data sets. Our experimental results, obtained using a variety of algorithms for endmember extraction, unconstrained and constrained linear unmixing, and nonlinear unmixing, indicate that the incorporation of spatial constraints can be beneficial in order to improve automatic endmember extraction from the input data and unconstrained and constrained linear spectral unmixing based on endmembers derived using spectral information only. Further experiments are necessary in order to fully substantiate the impact of spatial constraints on nonlinear spectral unmixing, a topic in which machine learning methods can provide highly relevant contributions. We anticipate that the full adaptation of soft classifiers such as support vector machines to sub-pixel analysis (e.g., via multi-regression) may push the frontiers of hyperspectral imaging to new application domains.

6. REFERENCES

[1] J. B. Adams, M. O. Smith, and P. E. Johnson, "Spectral mixture modeling: a new analysis of rock and soil types at the Viking Lander 1 site," *Journal of Geophysical Research*, vol. 91, pp. 8098–8112, 1986.

[2] N. Keshava and J. F. Mustard, "Spectral unmixing," *IEEE Signal Processing Magazine*, vol. 19, no. 1, pp. 44–57, 2002.

[3] A. Plaza, P. Martinez, R. Perez, and J. Plaza, "A quantitative and comparative analysis of endmember extraction algorithms from hyperspectral data," *IEEE Trans. Geosci. Remote Sens.*, vol. 42, no. 3, pp. 650–663, 2004.

[4] D. Heinz and C.-I Chang, "Fully constrained least squares linear mixture analysis for material quantification in hyperspectral imagery," *IEEE Trans. Geosci. Remote Sens.*, vol. 39, pp. 529–545, 2001.

[5] J. W. Boardman, F. A. Kruse, and R. O. Green, "Mapping Target Signatures Via Partial Unmixing of Aviris Data," *Proc. JPL Airborne Earth Sci. Workshop*, pp. 23–26, 1995.

[6] J. C. Harsanyi and C.-I Chang, "Hyperspectral image classification and dimensionality reduction: orthogonal subspace projection," *IEEE Trans. Geosci. Remote Sens.*, vol. 32, no. 4, pp. 779–785.

[7] M. E. Winter, "N-FINDR: an algorithm for fast autonomous spectral end-member determination in hyperspectral data," *Proc. SPIE Spectrometry V*, vol. 3753, pp. 266–277, 2003.

[8] R. A. Neville, K. Staenz, T. Szeredi, J. Lefebvre, and P. Hauff, "Automatic endmember extraction from hyperspectral data for mineral exploration," *Proc. 21st Canadian Symp. Remote Sens.*, pp. 21–24, 1999.

[9] J. A. Richards and X. Jia, *Remote Sensing Digital Image Analysis: An Introduction*, Springer, 2006.

[10] A. Plaza, P. Martinez, R. Perez, and J. Plaza, "Spatial/spectral endmember extraction by multidimensional morphological operations," *IEEE Trans. Geosci. Remote Sens.*, vol. 40, no. 9, pp. 2025–2041, 2002.

[11] A. Plaza, P. Martinez, J. Plaza, and R. Perez, "Dimensionality reduction and classification of hyperspectral image data using sequences of extended morphological transformations," *IEEE Trans. Geosci. Remote Sens.*, vol. 43, no. 3, pp. 466–479, 2005.

[12] C.-I Chang and Q. Du, "Estimation of number of spectrally distinct signal sources in hyperspectral imagery," *IEEE Trans. Geosci. Remote Sens.*, vol. 42, no. 3, pp. 608–619, 2004.